LETTERS

Temporal targeting of tumour cells and neovasculature with a nanoscale delivery system

Shiladitya Sengupta[1]*, David Eavarone[1]*, Ishan Capila[1], Ganlin Zhao[1], Nicki Watson[3], Tanyel Kiziltepe[2] & Ram Sasisekharan[1]

In the continuing search for effective treatments for cancer, the emerging model is the combination of traditional chemotherapy with anti-angiogenesis agents[1] that inhibit blood vessel growth. However, the implementation of this strategy has faced two major obstacles. First, the long-term shutdown of tumour blood vessels by the anti-angiogenesis agent can prevent the tumour from receiving a therapeutic concentration of the chemotherapy agent. Second, inhibiting blood supply drives the intra-tumoural accumulation of hypoxia-inducible factor-1α (HIF1-α); overexpression of HIF1-α is correlated with increased tumour invasiveness and resistance to chemotherapy[2–5]. Here we report the disease-driven engineering of a drug delivery system, a 'nanocell', which overcomes these barriers unique to solid tumours. The nanocell comprises a nuclear nanoparticle within an extranuclear pegylated-lipid envelope, and is preferentially taken up by the tumour. The nanocell enables a temporal release of two drugs: the outer envelope first releases an anti-angiogenesis agent, causing a vascular shutdown; the inner nanoparticle, which is trapped inside the tumour, then releases a chemotherapy agent. This focal release within a tumour results in improved therapeutic index with reduced toxicity. The technology can be extended to additional agents, so as to target multiple signalling pathways or distinct tumour compartments, enabling the model of an 'integrative' approach in cancer therapy.

Although the inhibition of angiogenesis is an elegant concept in cancer therapy[1], there are concerns about its implementation. Anti-angiogenesis therapy-induced tumoural hypoxia upregulates genes[2] that can significantly reduce the pro-apoptotic effect of chemotherapy[3] leading to 'reactive resistance'[4,5]. Furthermore, the activation of the hypoxic response can enhance the metastatic and invasive potential of tumour cells[6,7], although this has not been resolved clinically[8]. We reasoned that the optimal strategy to overcome these limitations is to sequentially expose the tumour to cytotoxic agents after a vascular shutdown induced by anti-angiogenesis therapy. However, two issues complicate this approach. First, the suppression of tumour growth requires long-term administration of angiogenesis inhibitors, whereas chemotherapy is usually given in short treatment cycles[9]. Second, the chronic administration of an anti-angiogenesis agent impairs blood flow inside the tumour microenvironment, precluding the intra-tumoural build-up of a therapeutically effective concentration of the chemotherapeutic agent.

To address this challenge we designed a novel delivery system, termed a nanocell, comprising a nanoscale pegylated-phospholipid block-copolymer envelope coating a nuclear nanoparticle. A chemotherapeutic agent is conjugated to the nanoparticle and an anti-angiogenesis agent is trapped within the lipid envelope. We proposed

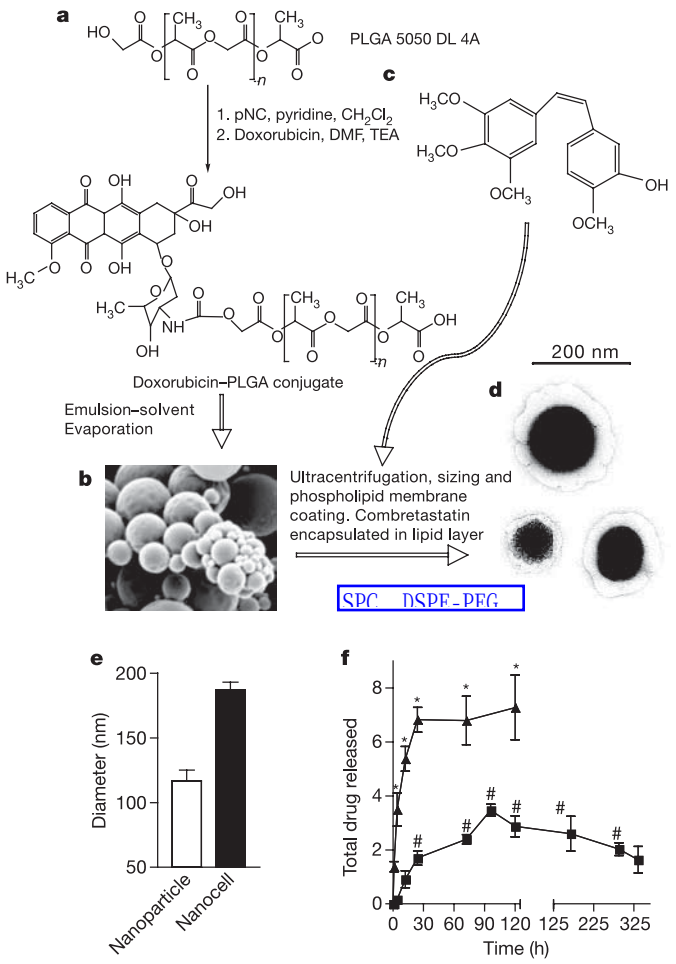

Figure 1 | Synthesis and characterization of a combretastatin–doxorubicin nanocell. a, Diagram of conjugation reactions between doxorubicin and PLGA 5050. DMF, dimethylformamide; pNC, p-nitrophenyl-chloroformate; TEA, triethylamine. **b**, Scanning electron micrograph of heterogeneous nanoparticles. **c**, Combretastatin is encapsulated in the lipid envelope. **d**, Transmission electron micrograph of the cross-section of three nanocells shows the dark nuclear nanoparticle within the phospholipid block-copolymer envelope. **e**, Dynamic light scattering shows that nanoparticles of defined sizes were used for encapsulation within the envelope. **f**, Physicochemical release kinetics shows the temporal release of combretastatin (triangles, scale in 10^2 μg) and doxorubicin (squares, scale in μg). Results are means ± s.e.m. ($n = 4$). The error is small where not visible. Asterisk, $P < 0.002$; hash, $P < 0.001$.

[1]Biological Engineering Division and [2]Department of Chemistry, Massachusetts Institute of Technology, Cambridge, Massachusetts 02139, USA. [3]Whitehead Institute for Biomedical Research, Cambridge, Massachusetts 02142, USA.
*These authors contributed equally to this work.

that the disruption of this envelope inside a tumour would result in a rapid deployment of the anti-angiogenesis agent, leading to vascular collapse and the intra-tumoural trapping of the nanoparticles. The subsequent slow release of the cytotoxic agent from the nanoparticle should then kill the tumour cells.

As a proof of concept, we selected doxorubicin and combretastatin-A4 as the cytotoxic agent and the anti-angiogenesis drug, respectively. Doxorubicin induces apoptosis by intercalating with the DNA, causing scission[10]. Combretastatin causes a rapid vascular shutdown inside a tumour by disrupting the cytoskeletal structures[11].

The nanoparticles were fabricated from the biodegradable and nonbioactive copolymer poly-(lactic-co-glycolic) acid (PLGA)[12]. Doxorubicin was conjugated to PLGA (Fig. 1a) to achieve a slow release profile, distinct from the characteristic 'burst' release associated with nanoparticles. *In vitro* cell culture studies revealed a shift in the concentration–effect curve of the doxorubicin–PLGA conjugate, for which the concentration giving half-maximal response (EC_{50}) was about 10.59 μg, compared with free doxorubicin ($EC_{50} \approx 5.93$ μg; Fig. 2c). This shift in the concentration–effect curve indicates that the doxorubicin–PLGA oligomers are inactive and have to degrade further into bioactive doxorubicin–PLGA fragments and free drug, which is consistent with earlier reports[13]. Although there was heterogeneity in the sizes of nanoparticles synthesized (Fig. 1b), we isolated a homogeneous population of nanoparticles between 80–120 nm (Fig. 1e).

To synthesize the nanocell, these nanoparticles were nucleated inside a nanoscale phospholipid block-copolymer envelope composed of 2,000-Da poly-(ethylene glycol) distearoylphosphatidylethanolamine (PEG-DSPE), phosphatidylcholine and cholesterol, in an optimal ratio with combretastatin. The selection of combretastatin, a lipophilic *cis*-stilbene (Fig. 1c), allowed optimal loading by partitioning into the lipid bilayer. Transmission electron microscopy showed the ultrastructure as being similar to a biological cell—a

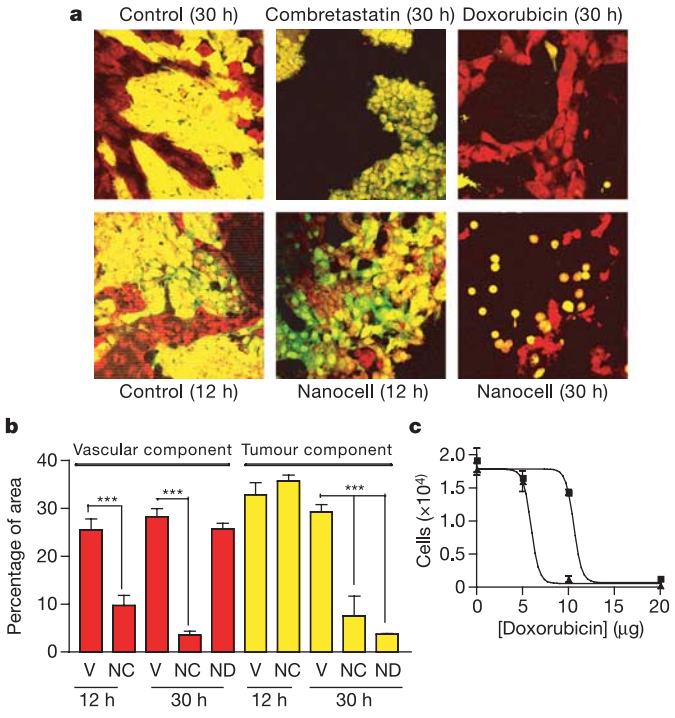

Figure 2 | Bioassay of the nanocell with a GFP-positive melanoma–endothelial cell three-dimensional co-culture system. a, Micrographs showing the effect of treatments on melanoma (yellow) or endothelium (red). **b**, Stereological quantification of the result. Treatment with nanocells (NC) results in temporal ablation of vasculature followed by destruction of the tumour cells. Liposomal combretastatin (250 μg ml^{-1}) (L[C]) and doxorubicin-conjugated nanoparticles (ND) (20 μg ml^{-1} doxorubicin) results in selective loss of vasculature and tumour respectively. Results are means ± s.e.m. from three independent experiments. V, vehicle. Three asterisks, $P < 0.001$ (analysis of variance with Bonferroni's post-hoc test). **c**, Concentration–effect curve of free doxorubicin (triangles) and PLGA-conjugated doxorubicin (squares) on B16/F10 cells. Results are means ± s.e.m. for two independent experiments.

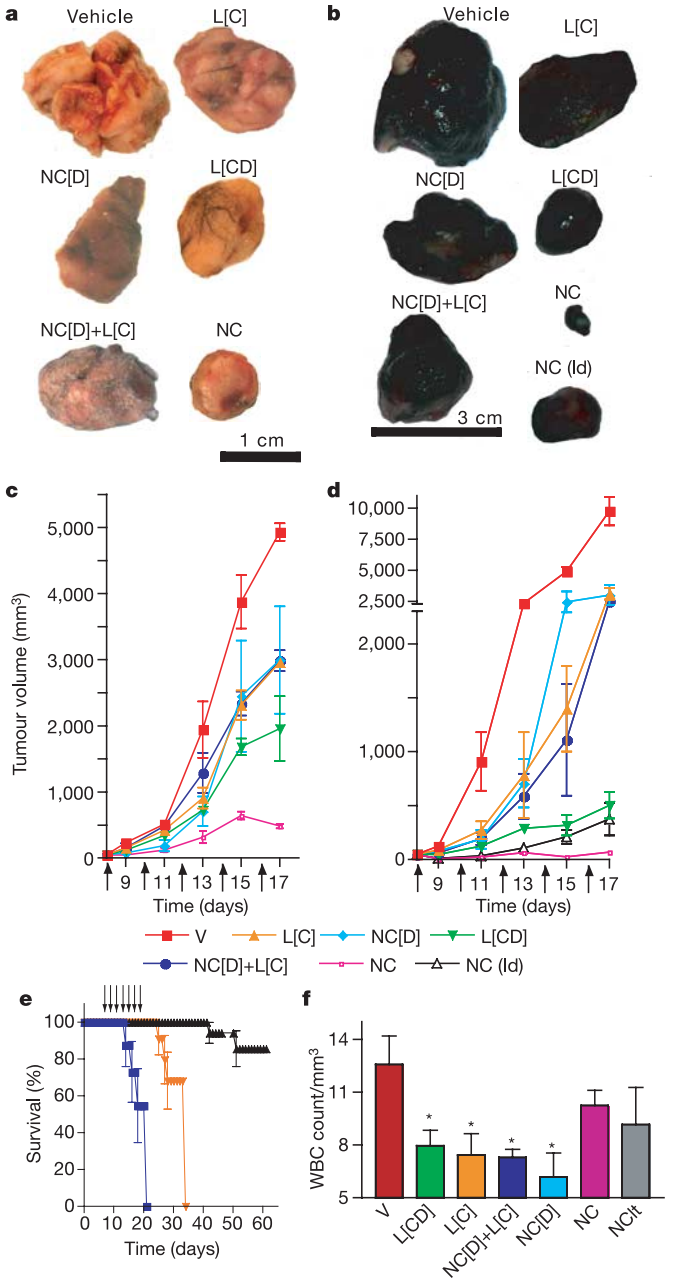

Figure 3 | Nanocell therapy inhibits B16/F10 melanoma and Lewis lung carcinoma growth. a, b, Excised Lewis lung carcinoma (**a**) and B16/F10 melanoma (**b**) comparing the effects of NC and the effects of nanocells with NC[D], L[C], co-injection of NC[D] + L[C], L[CD] and a lower dose (ld) of NC. Control groups received saline. **c**, **d**, Tumour volume in different treatment groups for Lewis lung carcinoma (**c**) and B16/F10 carcinoma (**d**). Results are means ± s.e.m. V, vehicle. **e**, Kaplan–Meier survival graph showing that treatment with NC significantly increases the lifespan: blue squares, vehicle; black triangles, NC; orange triangles, L[CD]. **f**, The effect of different treatments on the white blood cell (WBC) counts. Results are means ± s.e.m. Error is small where hidden. Arrows represent drug administration. *$P < 0.05$ vs. vehicle (V).

nuclear core surrounded by a lighter lipid membrane—hence the metaphor 'nanocell' (Fig. 1d). The size of the nanocells ranged between 180 and 200 nm in diameter (Fig. 1e).

To evaluate the nanocell physicochemically, we quantified the release kinetics for each drug. We observed a rapid release of combretastatin, reaching significant levels within 12 h. In contrast, the doxorubicin–PLGA oligomer was found to degrade into smaller doxorubicin–PLGA fragments and free doxorubicin significantly more slowly (Fig. 1f), extending over 15 days. This slow release underlines the shift in the concentration–effect curves, the EC_{50} being calculated at a time before the complete breakdown of the drug–polymer conjugate.

To correlate the temporal-release kinetics with the pathophysiology, we harnessed a tumour-endothelium co-culture bioassay[14]. The co-cultures were exposed to different treatments for defined periods, after which they were evaluated by dual-fluorescence confocal microscopy. As shown in Fig. 2, prolonged (30 h), but not short (12 h), incubation of the co-culture with doxorubicin-conjugated nanoparticles, alone, resulted in a complete ablation of the tumour cells without affecting the endothelial cells. This was consistent with the results obtained with free doxorubicin[14]. In contrast, incubation with combretastatin-encapsulated liposomes resulted in a rapid collapse of the vascular network without affecting the tumour cells. In the nanocell-treated groups, collapse of the vasculature was evident as early as 12 h, at which time point the tumour cells remained unaffected. A complete ablation of the co-culture was achieved by 30 h, which is consistent with the kinetics profile of the drug release rate. Although this release profile may not mimic the *in vivo* state, the close similarity of *ex vitro* release profiles in hypoxic-tumour cell lysate and PBS, together with the bioassay results, emphasizes that a similar release pattern over time would be functional in the acidic microenvironment of the tumour.

To validate the therapeutic efficacy of this treatment, we randomly sorted mice bearing established (green fluorescent protein (GFP)-positive) B16/F10 melanomas or Lewis lung carcinoma into six groups and treated each group with one of the following: PBS (control); nanocells containing doxorubicin nanoparticles but lacking combretastatin (NC[D]); combretastatin-encapsulated liposomes (L[C]); co-administration of NC[D] + L[C]; nanocells containing both doxorubicin and combretastatin (NC); and a simple liposomal system encapsulating both doxorubicin and combretastatin (L[CD]). A separate melanoma-bearing group received half the dose of NC. The mice injected with PBS formed large tumours by day 17 (the day after the last injection), and consequently were killed. The animals in the other groups were also killed at the same time point to evaluate the effect of the treatments on tumour pathology. In a separate experiment, another group of animals was given seven cycles of treatment with NC to evaluate the effect over a longer period.

As shown in Fig. 3, both the L[C] and NC[D] groups showed tumour inhibition compared with the PBS-treated group. The NC[D] + L[C] treatment group had only a negligible improvement over either of the treatments alone, which could arise from the preclusion of NC[D] after chronic administration of the anti-angiogenic agent. In contrast, L[CD] treatment induced a greater inhibition than NC[D] + L[C], possibly from the simultaneous release of free doxorubicin and combretastatin. A greater exposure to the cytotoxic agent at the acute phases of the therapy, resulting from the normalization of the tortuosity of tumour vessels[15], has

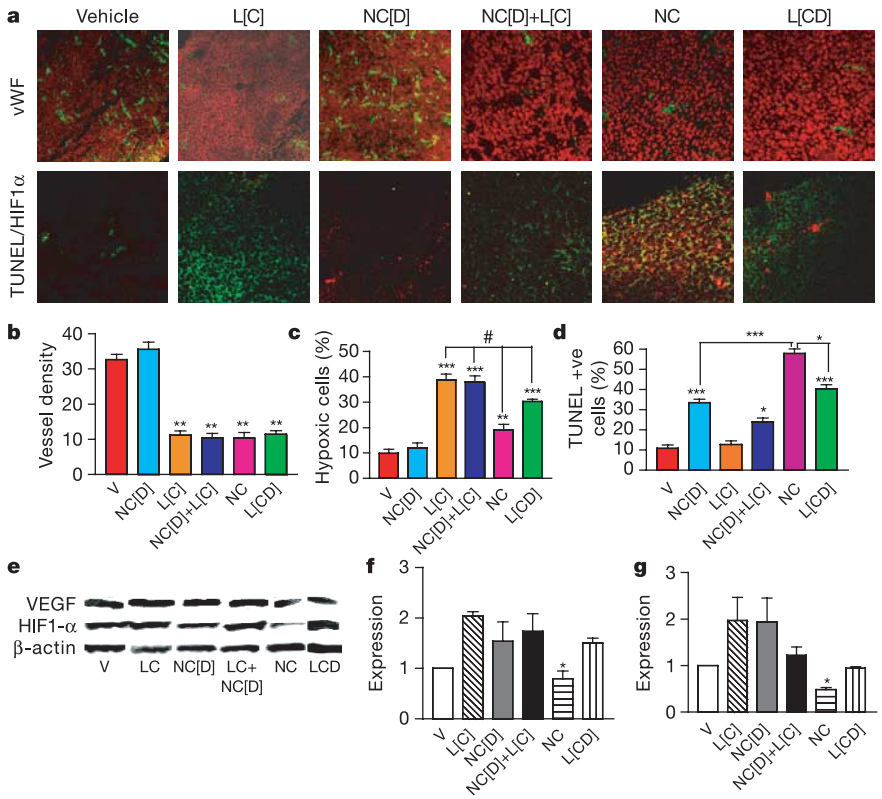

Figure 4 | Effect of nanocell treatment on tumour vasculature and apoptosis. a, Top: cross-section of tumours immunostained for vWF, an endothelial marker. Bottom: tumours TUNEL-labelled for apoptosis with the use of Texas red-labelled nucleotide, and co-stained with an anti-HIF1-α antibody labelled by FITC. **b–d**, Graphs showing tumour vessel density (**b**), hypoxia (**c**) and apoptosis (**d**). Results are means ± s.e.m. ($n = 3$). Asterisk, $P < 0.05$; two asterisks, $P < 0.01$; three asterisks, $P < 0.001$; all compared with controls (analysis of variance with Newman–Keul's post-hoc test). **e**, Western blots showing the effect of different treatments on the levels of HIF1-α and VEGF;. **f**, **g**, Graphs of levels of HIF1-α (**f**) and VEGF (**g**), normalized to β-actin; expression is shown relative to vehicle, normalized to 1. Results are means ± s.e.m. Asterisk, $P < 0.05$ compared with other combretastatin-treated groups.

been reported to underlie such an outcome. Another explanation could be that low-dose (that is, 'metronomic') chemotherapy can also exert an anti-angiogenetic effect[16]. However, the NC-treated groups, when compared directly with the equivalent doses of the NC[D], L[C], NC[D] + L[C] and L[CD] groups, had a distinctly superior outcome. NC treatment-induced inhibition of tumour growth was dose-dependent, although melanoma was more susceptible than lung carcinoma. Furthermore, there was a significant increase in the lifespan of the NC-treated animals (Fig. 3e). These observations bring out two issues. First, it is well known that tumour cell response to chemotherapy is a function of the chemotherapeutic agent. As observed here, the greater susceptibility of melanoma than the Lewis lung carcinoma to this current drug combination is consistent with this view. Second, the effectiveness of a chemotherapeutic agent is likely to be a function of signalling pathways and the responses to extracellular signalling from the heterotypic environment that impinge on the tumour cells. This underscores the need to develop chemotherapeutic approaches while keeping in perspective the different compartments of distinct tumours.

To dissect the mechanism of action, we immunostained tumour cross-sections for an angiogenesis marker, von Willebrand factor (vWF). As shown in Fig. 4a, c, the L[C] group induced a more than 50% loss in vasculature compared with PBS-treated controls. There was no difference in the vessel density between the groups treated with L[C], L[CD], NC and the NC[D] + L[C]. NC[D] had no effect on the tumour vasculature, indicating that 'metronomic' dose anti-angiogenesis was not the underlying cause for the enhanced efficacy observed with nanocells.

We next evaluated the tumours for apoptosis by using TdT-mediated dUTP nick end labelling (TUNEL) staining, staining the same sections simultaneously for HIF1-α expression. As shown in Fig. 4a, d, e, NC[D] treatment induced significant apoptosis in the tumour without any increase in the expression of HIF1-α. L[C] treatment did not induce apoptosis, nor did it potentiate the effect of NC[D] when both were injected together. A possible explanation for this observation could be attributed to the accumulation of HIF1-α, which can upregulate pro-survival growth factors[7]. In contrast, administration of NC significantly increased the percentage of TUNEL-positive cells in the tumour in comparison with NC[D] alone, and also disconnected the expressions of HIF1-α and vascular endothelial growth factor (VEGF) in comparison with other anti-angiogenesis-treated groups (Fig. 4e–g), possibly arising from a focal build-up of doxorubicin inside the tumour, leading to increased apoptosis.

Analysis of the white blood cell count, which is highly susceptible to cytotoxic agents, showed that treatment with NC resulted in the least systemic toxicity (Fig. 3f), consistent with the intra-tumourally restricted release of the cytotoxic agent arising from the vascular shut-down. To confirm the enhanced uptake into the tumour, we fabricated nanocells with fluorescein and monitored the level of the dye in the tumour and other highly vascular organs. The nanocells were detected within 5 h in all the vascularized tissues in equilibrium with the levels in the blood, and preferential accumulation of the nanocells in the tumours was evident at 24 h, with a concomitant fall in the serum level (Supplementary Fig. 2). This selective uptake into the tumour could arise from increased residence time in the circulation as a result of pegylation-induced reduction in immunogenicity[17]. Furthermore, the unique 'leakiness' of the tumour vessels, which, unlike physiological vasculature, have pores that are 400–600 nm in diameter[18], enhances the permeability and retention of the nanocells fabricated in this study. Additionally, the anti-angiogenesis agent-induced decrease in hydrostatic pressure gradient across the vascular wall could explain the increased accumulation at 24 h compared with earlier time points[19]. Although further studies are needed to dissect out these effects, the reduced toxicity and enhanced anti-tumour anti-metastatic effects (Supplementary Fig. 3) emphasizes the advantages of the mechanism-based design of the system.

Several components of the nanocell approach can facilitate future therapy in humans. First, the nuclear arrangement of cytotoxic agent-conjugated nanoparticle and the encapsulation of the anti-angiogenesis agent in the surrounding phospholipid block-copolymer envelope enables temporal targeting of the tumour vasculature, resulting in the intra-tumoural trapping of the nanoparticles. Second, the resultant slow release and focal build-up of the cytotoxic agent within the tumour allows a prolonged exposure and an increase in the apoptotic potential, which can overcome hypoxia-induced reactive resistance. Third, although we show here a selective tumour uptake, we recognize that these vehicles can be further specifically targeted to tumour vasculature by using probes that recognize specific molecular signatures on the vasculature[20]. Thus, the nanocell concept enables a significant advance in cancer therapy over current approaches. This platform technology supports the paradigm shift from a 'reductive' to an 'integrative' approach in cancer therapy[21].

METHODS

Synthesis and characterization of nanocells. Activated PLGA was dissolved in dimethylformamide and reacted with doxorubicin and triethylamine at room temperature (20 °C) under a nitrogen atmosphere (stoichiometric molar ratio of activated PLGA:doxorubicin:triethylamine, 1:1:4)[13]. Nanoparticles were formulated from the PLGA copolymer–doxorubicin conjugates by using an emulsion–solvent evaporation technique. For scanning electron microscopy, dehydrated nanoparticles were coated with gold on a carbon grid. They were analysed using a Jeol electron microscope (magnification × 3,700). Nanoparticle size fractions were recovered by ultracentrifugation at 10,000 *g*, 25,000 *g* and 50,000 *g*, which also removed free doxorubicin from the PLGA–doxorubicin conjugates. The smallest fraction was extruded through a membrane (pore size 100 nm) to obtain nanoparticles for encapsulation within nanocells. Phosphatidylcholine:cholesterol:PEG-DSPE (2:1:0.2 molar ratio) lipid membranes were prepared by dissolving the lipids in chloroform in a round-bottomed flask. Combretastatin A4 was added at a 0.9:1 drug:lipid molar ratio. To fabricate the nanocells, doxorubicin-conjugated nanoparticles were added to the aqueous lipid resuspension buffer, which was extruded through a membrane (pore size 200 nm). Sizing was performed by dynamic light scattering and transmission electron microscopy. For further details see Supplementary Fig. 4.

Cell culture studies. B16/F10 cells were plated at a concentration of 5×10^4 cells per well and left to grow for 24 h in 5% fetal calf serum. The cells were exposed to increasing concentrations of free or nanoparticle-conjugated doxorubicin and incubated for 48 h, after which the cells were counted with the Trypan blue exclusion method. EC_{50} was calculated by curve-fitting.

Release kinetics characterization. Drug-loaded nanocells were suspended in 1 ml of PBS buffer or hypoxic-cell lysate and sealed in a dialysis bag (molecular mass cut-off 10 kDa). The dialysis bag was incubated in 20 ml of PBS buffer at 37 °C with gentle shaking. Aliquots were extracted from the incubation medium at predetermined intervals, and released drug was quantified by reverse-phase HPLC with a C_{18} column, using a linear gradient of acetonitrile and water eluents. For further details see Supplementary Information.

***In vitro* tumour–endothelium co-culture studies.** The co-culture of GFP-positive B16/F10 melanoma with human umbilical vein endothelial cells on a three-dimensional Matrigel matrix was exposed to different treatments. The cells were fixed with 4% paraformaldehyde, incubated with propidium iodide and analysed with a confocal microscope. Quantification was performed with a planimetric point-count method using a 224-intersection point square reticulum. Data were expressed as the ratio of each component to the total area covered by cells. For further details see Supplementary Information.

***In vivo* tumour studies.** GFP-positive BL6/F10 melanoma cells (3×10^5) or Lewis lung carcinoma cells (2.5×10^5) were implanted in male C57/BL6 mice. Treatment was started when the tumours reached 50 mm^3 in volume. Each formulation was prepared, quantified and diluted so that 100 μl (intravenous) was equivalent to 50 mg kg^{-1} combretastatin and 500 μg kg^{-1} doxorubicin. The animals were killed at defined time points, and the tumours were excised for histopathology. Simultaneously, 1 ml of blood was drawn through cardiac puncture and analysed for a toxicity profile of the treatment regimens.

Tissue distribution studies. Nanocells were fabricated with fluorescein dye and injected into tumour-bearing mice. The animals were killed at 5, 10 and 24 h after injection. Serum, tumour, liver, lungs and spleen were collected during necropsy, and fluorescein was extracted from these tissues with methanol, detected with a fluorescence plate reader, and normalized to the tissue weight. In another study, nanocells were fabricated with Quantum Dots in the core, and injected intravenously into tumour-bearing mice. The animals were killed at

different time points, and the highly vascular organs were extracted during necropsy. The tissue sections (30 μm thick) were immunostained to delineate the blood vessels. Confocal images were captured at 512 pixels × 512 pixels resolution, with excitation using a 488-nm laser line and emissions at the fluorescein isothiocyanate (FITC)/rhodamine wavelengths. Depth-coding was performed with LSM510 software.

Immunohistology. For analysis of tumour vasculature, permeabilized cryosections of the tumours were immunoprobed for vWF, an endothelial cell marker. For study of apoptosis, TUNEL staining was performed with Texas red-labelled nucleotide in accordance with the manufacturer's instructions (Roche). The same sections were also stained simultaneously for HIF1-α, using appropriate primary and FITC-labelled secondary antibodies. Images were captured with a Leica LSM510 confocal microscope at a 512 pixels × 512 pixels resolution. For quantifying metastatic nodes, the liver and lungs were harvested from the animals during necropsy, fixed in paraformaldehyde and embedded in paraffin. Thin sections were stained with haematoxylin/eosin and imaged with a Zeiss LSM510 confocal microscope with FITC/rhodamine filters. Metastatic nodes were quantified by counting the number of yellow foci in each section. For further details see Supplementary Information.

Western blotting. Tissue samples were lysed in sample buffer and resolved on a 4–12% gradient SDS–polyacrylamide-gel electrophoresis gel. The proteins were transferred to a nitrocellulose membrane, blocked, and probed with the appropriate primary antibodies and secondary horseradish peroxidase-labelled antibodies. Proteins were detected by chemiluminescence and quantified with a Kodak 2000 gel-imaging system.

Received 30 December 2004; accepted 10 May 2005.

1. Kerbel, R. S. & Kamen, B. A. The anti-angiogenic basis of metronomic chemotherapy. *Nature Rev. Cancer* **4,** 423–436 (2004).
2. Semenza, G. L. Surviving ischemia: adaptive responses mediated by hypoxia-inducible factor 1. *J. Clin. Invest.* **106,** 809–812 (2000).
3. Tran, J. *et al.* A role for survivin in chemoresistance of endothelial cells mediated by VEGF. *Proc. Natl Acad. Sci. USA* **99,** 4349–4354 (2002).
4. Yu, J. L., Rak, J. W., Coomber, B. L., Hicklin, D. J. & Kerbel, R. S. Effect of p53 status on tumour response to antiangiogenic therapy. *Science* **295,** 1526–1528 (2002).
5. Blagosklonny, M. V. Antiangiogenic therapy and tumour progression. *Cancer Cell* **5,** 13–17 (2004).
6. Pennacchietti, S. *et al.* Hypoxia promotes invasive growth by transcriptional activation of the met protooncogene. *Cancer Cell* **3,** 347–361 (2003).
7. Rofstad, E. K. *et al.* Hypoxia promotes lymph node metastasis in human melanoma xenografts by up-regulating the urokinase-type plasminogen activator receptor. *Cancer Res.* **62,** 1847–1853 (2002).
8. Kieran, M. W., Folkman, J. & Heymach, J. Angiogenesis inhibitors and hypoxia. *Nature Med.* **9,** 1104 (2003).
9. Kerbel, R. & Folkman, J. Clinical translation of angiogenesis inhibitors. *Nature Rev. Cancer* **2,** 727–739 (2002).
10. Chabner, B. A., *et al. Goodman and Gilman's The Pharmacological Basis of Therapeutics* 9th edn (McGraw-Hill, 1996).
11. Tozer, G. M., Kanthou, C., Parkins, C. S. & Hill, S. A. The biology of the combretastatins as tumour vascular targeting agents. *Int. J. Exp. Pathol.* **83,** 21–38 (2002).
12. Miklos, A. G., Lyman, M. D., Freed, L. E. & Langer, R. Wetting of poly(L-lactic acid) and poly(D-lactic-co-glycolic acid) foams for tissue culture. *Biomaterials* **15,** 55–58 (1994).
13. Yoo, H. S., Oh, J. E., Lee, K. H. & Park, T. G. Biodegradable nanoparticles containing doxorubicin-PLGA conjugate for sustained release. *Pharm. Res.* **16,** 1114–1118 (1999).
14. Sengupta, S., Kiziltepe, T. & Sasisekharan, R. A dual-colour fluorescence imaging-based system for the dissection of antiangiogenic and chemotherapeutic activity of molecules. *FASEB J.* **18,** 1565–1567 (2004).
15. Jain, R. K. Normalizing tumour vasculature with anti-angiogenic therapy: a new paradigm for combination therapy. *Nature Med.* **7,** 987–989 (2001).
16. Hanahan, D., Bergers, G. & Bergsland, E. Less is more, regularly: metronomic dosing of cytotoxic drugs can target tumour angiogenesis in mice. *J. Clin. Invest.* **105,** 1045–1047 (2000).
17. Allen, T. M. Ligand-targeted therapeutics in anticancer therapy. *Nature Rev. Drug Discov.* **2,** 750–763 (2002).
18. Yuan, F. *et al.* Vascular permeability in a human tumour xenograft: molecular size dependence and cutoff size. *Cancer Res.* **55,** 3752–3756 (1995).
19. Tong, R. T. *et al.* Vascular normalization by vascular endothelial growth facor receptor-2 blockade induces a pressure gradient across the vasculature and improves drug penetration in tumors. *Cancer Res.* **64,** 3731–3736 (2004).
20. Arap, W. *et al.* Steps toward mapping the human vasculature by phage display. *Nature Med.* **8,** 121–127 (2002).
21. Hanahan, D. & Weinberg, R. A. The hallmarks of cancer. *Cell* **100,** 57–70 (2000).

Supplementary Information is linked to the online version of the paper at www.nature.com/nature.

Acknowledgements We thank S. R. Kabir, K. Holley and G. T. Franzesi for assistance.

Author Information Reprints and permissions information is available at npg.nature.com/reprintsandpermissions. The authors declare no competing financial interests. Correspondence and requests for materials should be addressed to R.S. (rams@MIT.edu).